Kinematics of mono- and bidisperse granular flow in quasi-two-dimensional bounded heaps

Yi Fan[1,†], Paul B. Umbanhowar[1], Julio M. Ottino[1,2,3], and Richard M. Lueptow[1,3,‡]

[1] *Department of Mechanical Engineering, Northwestern University, Evanston, Illinois 60208, USA*
[2] *Department of Chemical and Biological Engineering, Northwestern University, Evanston, Illinois 60208, USA*
[3] *The Northwestern University Institute on Complex Systems (NICO), Northwestern University, Evanston, IL 60208, USA*

Quasi-two-dimensional (2D) bounded heap flow is a useful model for granular flows in many industrial processes and natural phenomena. It belongs to the family of free surface flows - inclined chute flow, rotating tumbler flow, and unbounded heap flow - but is different from all of them in that the uniform deposition of particles onto the static bed results in the uniform rise of the heap and presumably simpler kinematics. The kinematics, however, is only imperfectly understood. We performed discrete element method (DEM) simulations to study mono- and bidisperse granular flows in quasi-2D bounded heaps. The experimentally validated computational results show a universal functional form for the streamwise velocity profile for both mono- and bidisperse systems when velocities and coordinates are scaled by the local surface velocity and the local flowing layer thickness. This holds true regardless of streamwise location, feed rate, particle size distribution and, most surprisingly, for bidisperse flows, the local particle concentration. We find that the local surface velocity decreases linearly in the streamwise direction, while the flowing layer thickness remains nearly constant with both quantities depending only on local flow rate and local mean particle diameter. We show also that the velocity profile normal to the overall flow, which is important in understanding segregation, can be predicted analytically from the streamwise velocity and matches the simulation results well.

1. Introduction

Understanding the flow of non-cohesive particles, common in many industrial and geophysical situations, is challenging because no universal governing equations like the Navier-Stokes equations for Newtonian fluid flow exist for granular flow. As a result, several canonical model flows including heap flow, rotating tumbler flow, and chute flow are frequently studied to better grasp the physics of granular flows. Here we study bounded heap flow in which, unlike unbounded heap flow, an endwall limits the downstream extent of the heap and forces the free surface height to increase with time. This flow geometry is shown in figure 1(a). Typically, to study the flow a quasi-two-dimensional (2D) experimental apparatus is used in which the spanwise extent is small (O(10) particle diameters). In addition, most experiments consider a half heap where grains are fed from the side as shown in figure 1(a).

Bounded heap flow differs in several key aspects from other canonical quasi-2D free surface granular flows including rotating tumblers, unbounded heaps, and inclined chutes (GDR MiDi, 2004) (figure 1(b-d)). For sufficiently large volumetric feed rate Q, the surface flow is continuous (non-avalanching) and, because flowing grains are stopped by the endwall at the downstream end of the heap, the free surface rises steadily and uniformly along the length of the heap at a rise velocity, v_r. The local flow rate decreases linearly along the streamwise direction to zero at the downstream endwall due to deposition of particles into the static bed. This decrease of local flow rate induces a streamwise velocity gradient along the streamwise direction.

In contrast, in unbounded heap flow or inclined chute flow, there is no endwall to stop the flow, so the local flow rate remains constant along the streamwise direction and is fully developed (i.e. $du/dx = 0$, where u is the streamwise velocity and x is the streamwise direction). Furthermore, the free surface location is fixed in these systems, as shown in figure 1. There have been extensive studies of kinematics in unbounded heap flow and inclined chute flow, for both monodisperse systems (e.g. Savage & Hutter (1989); Lemieux & Durian (2000); Komatsu *et al.* (2001); Pouliquen & Forterre (2002); GDR MiDi (2004); Crassous *et al.* (2008);

[†]Email:yi-fan@northwestern.edu
[‡]Email:r-lueptow@northwestern.edu

Proc. R. Soc. A 1–16; doi: 10.1098/rspa.00000000
March 23, 2013

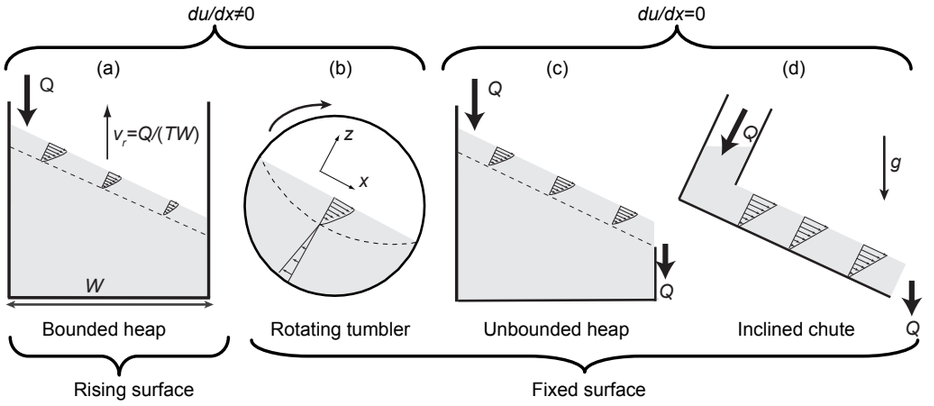

Figure 1. Four configurations of free surface flow in a quasi-two-dimensional geometry: (a) bounded heap, (b) rotating tumbler (c) unbounded heap, and (d) inclined chute. g is acceleration due to gravity and u is the streamwise velocity.

de Ryck *et al.* (2010) and references therein) and bidisperse systems (e.g. Goujon *et al.* (2007); Rognon *et al.* (2007); Wiederseiner *et al.* (2011); Tripathi & Khakhar (2011)). These studies indicate that the streamwise velocity decreases approximately linearly with depth from the surface through most of the flowing layer (shown schematically in figure 1(c-d)) and exponentially in the deepest regions of the flowing layer. The depth-averaged streamwise velocity $\overline{u}$ in the flowing layer and the thickness of the flowing layer δ are constant in the streamwise direction at a fixed feed rate Q, and increase as Q increases.

While flow in rotating tumblers is similar to bounded heap flow in that $\overline{u}$ varies in the streamwise direction (Khakhar *et al.*, 1997; Orpe & Khakhar, 2001; Bonamy *et al.*, 2002; Jain *et al.*, 2002), the location of the free surface in the rotating tumbler remains fixed, as in unbounded heap flow and inclined chute flow. Unlike heap and chute flows where a feed source Q is needed to sustain the flow, in a rotating tumbler particles periodically enter and leave the flowing layer as the tumbler rotates.

Compared to the extensive studies on the kinematics of other free surface flows (summarized in GDR MiDi (2004)), only a few studies (Boutreux *et al.*, 1998; Khakhar *et al.*, 2001) have investigated the kinematics of bounded heap flow. By assuming a constant depth-averaged streamwise velocity along the flowing layer at each feed rate, Boutreux *et al.* (1998) and Khakhar *et al.* (2001) concluded that the local thickness of the flowing layer decreases along the streamwise direction. However, details of the kinematics such as the profiles of both velocity components (in the streamwise and normal direction) and solids volume fraction at different locations along the streamwise direction were not measured. Here we use DEM simulation to better understand these important details of bounded heap flow.

In addition to considering monodisperse granular systems, we also examine the kinematics of bidisperse systems during heap flow due to its fundamental importance in driving segregation. Polydisperse granular materials tend to segregate during heap formation, often resulting in inhomogeneous final particle distributions. Heap segregation occurs in many contexts, particularly in industrial applications, and in most cases, the segregation is unwanted. Therefore, understanding the mechanisms of and developing a predictive model for segregation in heap flows is desirable. Previous studies on segregation of bidisperse mixtures of different-sized particles in quasi-2D bounded heap flow found three different final particle configurations: stratified in which there are layers of large and small particles (Baxter *et al.*, 1998; Makse *et al.*, 1997*a*,*b*; Gray & Hutter, 1997; Gray & Ancey, 2009; Benito *et al.*, 2013), segregated in which small particles form the central portion of the heap and large particles form the outer portion (Williams, 1963, 1968; Shinohara *et al.*, 1972; Drahun & Bridgwater, 1983; Thomas, 2000; Goyal & Tomassone, 2006; Rahman *et al.*, 2011), and mixed in which the particles do not segregate (Baxter *et al.*, 1998; Koeppe *et al.*, 1998). Our recent experiments (Fan *et al.*, 2012) showed that the transition between stratified and segregated states was controlled by the 2D feed rate ($q_0 = Q/T$, where T is the gap thickness between the two bounding side walls of the quasi-2D heap) while the transition between segregated and mixed states was determined by the heap rise velocity ($v_r = q/W$, where W is the horizontal width of the heap from the feed location to the outer bounding wall).

These different final particle configurations and the transitions between them are closely associated with the unique characteristics of the kinematics in bounded heap flow. For example, in a bounded heap, small particles percolate to the bottom of the flowing layer and deposit into the static bed, while large particles accumulate in the downstream region. The degree of segregation is influenced by the heap rise velocity (Fan *et al.*, 2012), presumably due to the velocity of small particle percolation through the depth of the flowing layer compared to the rise velocity. In contrast, in unbounded heaps or inclined chutes, small particles segregate to the bottom of the flowing layer but continue to flow until they reach the end of the flowing layer. In rotating tumblers, particles exit the flowing layer and remain in the same streamlines before re-entering the flowing layer. As a result, in these

flows only the segregation rate but not the degree of segregation of the final state is influenced by the flow rates (Ottino & Khakhar, 2000; Meier *et al.*, 2007), as is the case for bounded heap flow.

Local particle distributions for segregating bidisperse mixtures in bounded heap flow have been modeled by Shinohara *et al.* (1972) and Boutreux & de Gennes (1996) by incorporating the percolation/segregation model proposed by Williams (1963, 1968) and Bridgwater and colleagues (Cooke *et al.*, 1978; Bridgwater *et al.*, 1978; Drahun & Bridgwater, 1983) into a continuum framework. Although these two models are able to predict some general features of heap segregation/stratification (Makse *et al.*, 1997*a*; Goyal & Tomassone, 2006; Rahman *et al.*, 2011), the lack of details of concerning the kinematics in the bounded heap flow necessitates unverified assumptions (e.g. the collision model in Boutreux & de Gennes (1996) or the velocity ratio of different sub-layers Shinohara *et al.* (1972); Shinohara & Enstad (1990)) with fitting parameters determined from experiments or simulations. Characterizing the kinematics of segregating bidisperse particles is necessary to enable better segregation models for bounded heap flow.

In this research, we perform a computational study of quasi-2D bounded heap flow using the discrete element method to investigate the kinematics of both monodisperse and bidisperse systems. We examine the continuous flow regime in which the segregated state occurs (Fan *et al.*, 2012). The kinematics of intermittent avalanches, which can result in stratified states, is not examined here, though it has been explored in other studies (Lemieux & Durian, 2000; Abate *et al.*, 2007; Linares-Guerrero *et al.*, 2007). In §2, the simulation technique and geometry are introduced and comparisons with experiments are made to validate our simulations in terms of local particle distributions at steady state and velocity profiles in the flowing layers. In §3, kinematics for both monodisperse and bidisperse systems are presented, including velocity profiles in both the flow and normal directions, and the local thickness of the flowing layer at particle size ratios, R, from 1 to 3 (where R is the ratio of large particle diameter d_l to small particle diameter d_s) and a range of feed rates, Q. We find that at fixed R and Q the local surface streamwise velocity u_s and local mean shear rate $\dot{\gamma}$ decrease approximately linearly along the streamwise direction, while the thickness of the flowing layer δ remains roughly constant. We also find a scaling law that collapses all streamwise velocity profiles at different feed rates and particle size distributions onto a single curve. §4 presents our conclusions.

2. Simulation approach and experimental validation

2.1. Simulation method and geometry

The discrete element method (DEM) is used here to simulate quasi-2D bounded granular heap flow. In DEM simulations the translational and rotational motion of each particle are calculated by integrating Newton's second law. The forces between particles are repulsive and are non-zero only when particles are in contact. We used a linear-spring dashpot force model (Cundall & Strack, 1979; Schafer *et al.*, 1996; Ristow, 2000; Chen *et al.*, 2008) to calculate the normal force between two contacting particles. It consists of two parts: a normal elastic force and a normal viscous damping force such that $\boldsymbol{F}_{ij}^n = [k_n\epsilon - 2\gamma_n m_{eff}(\boldsymbol{V}_{ij}\hat{\boldsymbol{r}}_{ij})]\hat{\boldsymbol{r}}_{ij}$. Here ϵ and $\boldsymbol{V}_{ij} = \boldsymbol{V}_i - \boldsymbol{V}_j$ denote the overlap and relative velocity of two contacting particles i and j, respectively. $\hat{\boldsymbol{r}}_{ij}$ represents the unit vector in the normal direction between particles i and j, and $m_{eff} = \frac{m_i m_j}{m_i + m_j}$ is the reduced mass. k_n and γ_n characterize the stiffness and damping of the granular materials, respectively, and are related to the collision time Δt and restitution coefficient e by $\gamma_n = -\frac{\ln e}{\Delta t}$ and $k_n = [\left(\frac{\pi}{\Delta t}\right)^2 + \gamma_n^2]m_{eff}$ (Schafer *et al.*, 1996; Ristow, 2000). For the tangential force, a linear spring at the contact point between two particles provides a restoring force. If this restoring force is larger than the Coulomb friction force, the spring is "cut" and the force is sliding friction based on Coulomb's law. The tangential force can therefor be expressed as $\boldsymbol{F}_{ij}^t = -\min\left(|\mathrm{k_s}\beta|, |\mu \boldsymbol{F}_{\mathrm{ij}}^{\mathrm{n}}|\right)\mathrm{sgn}(\beta)\hat{\boldsymbol{s}}$. Here the tangential displacement β is given by $\beta(t) = \int_{t_s}^{t} \boldsymbol{V}_{ij}^s dt$ (Rapaport, 2002) where t_s is the initial contact time between two particles. $\boldsymbol{V}_{ij}^s$ is the relative tangential velocity of two particles and $\hat{\boldsymbol{s}}$ is the unit vector in the tangential direction. The tangential stiffness is $k_s = \frac{2}{7}k_n$ (Schafer *et al.*, 1996). The velocity-Verlet algorithm (Ristow, 2000) is used to update the positions and velocities of particles.

The quasi-2D bounded heap simulated here is sketched in figure 2. To save computational cost, we simulate only the steady filling stage, where the heap contacts the bounding endwall and rises steadily and uniformly, which is similar to the experimental setup of Drahun & Bridgwater (1983). To accomplish this, the bottom wall of the domain is inclined at an angle $\theta = 24^o$ to horizontal, which is slight less than the dynamic angle of repose α in our previous experiments (Fan *et al.*, 2012). Upon filling, particles in contact with the inclined bottom wall are immobilized to increase the effective wall friction similar to the physical situation where particles deposit on the heap and stop flowing. When the heap is sufficiently deep ($\sim$10 particle diameters) after an initial time period t_0 ($\approx 10 d_l/v_r$), the effect of the bottom wall on the flowing layer is negligible and the flow reaches a steady state comparable to our experiments. The dimensions of the simulated domain are the same as those in our previous experiments (Fan *et al.*, 2012): the width of the domain, W, is 0.46 m and the gap thickness between the front and back walls, T, is 0.013 m. Particles are fed into the left end of the domain 0.1 m above the bottom wall at a mass flow rate $\dot{m}$. The width of the feed zone, the initial velocity, and the packing density of the particles in the feed

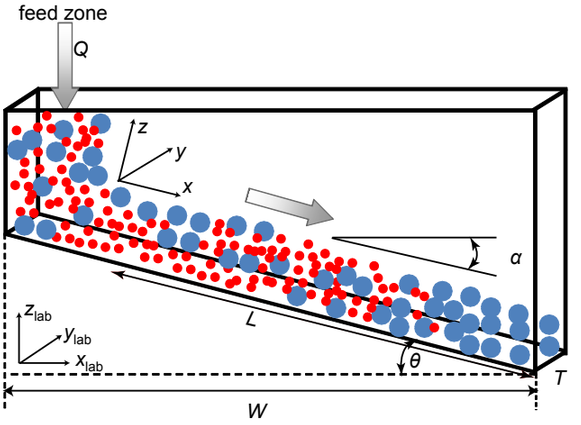

Figure 2. Sketch (not to scale) of a quasi-2D bounded heap with bottom wall inclined by θ. The heap width is W and the gap thickness is T. The length of the flowing layer from the downstream end of the feed zone to the bounding end wall is L. Two coordinates systems are used. $(x_{\rm lab}, y_{\rm lab}, z_{\rm lab})$ refers to the laboratory coordinate system with origin at the left front corner and (x, y, z) refers to a moving rotated coordinate system, where x denotes the streamwise direction, z denotes the direction normal to the flow, and y is the same as $y_{\rm lab}$. The origin is at the intersection of the free surface, the front wall, and the downstream edge of the feed zone.

stream are varied to achieve different $\dot{m}$. We performed several trial computational runs and found the kinematics and segregation insensitive to these feed parameters at constant $\dot{m}$.

The material density of the simulated particles $\rho = 2500$ kg/m^3 and restitution coefficient $e = 0.8$. The particle-particle and particle-wall friction coefficients are set to $\mu = 0.4$. Note that the side walls are frictional and flat to allow direct comparisons to experiments. To save computational time, the binary collision time is set to $\Delta t = 10^{-3}$ s, consistent with previous simulations (Chen *et al.*, 2011) and sufficient for modeling hard spheres (Silbert *et al.*, 2007) based on comparison with results for $\Delta t = 10^{-4}$ s. The integration time step is $\Delta t/100 = 1.0 \times 10^{-5}$ s to assure numerical stability. To prevent crystallization, the particles have a uniform size distribution with a variance of $(0.1d_i)^2$, where d_i is the mean particle diameter for each species i. There are up to one million particles in our simulations depending on $\dot{m}$ and particle size. Simulations typically are run for 15 to 100 seconds of physical time, and the initial time for reaching steady state t_0 is approximately 1/3 of the total simulation time.

As shown in figure 2, two different coordinate systems are used. The first is the fixed laboratory coordinate system $(x_{\rm lab}, y_{\rm lab}, z_{\rm lab})$ with origin at the left bottom corner of the domain, which is used to measure particle distributions of the final states. The second coordinate system (x, y, z) is rotated by the dynamic angle of repose α of the flowing particles and moves upward so that the $x-$axis is always at the free surface. It is used for the time-averaged kinematics in the flowing layer. The x-axis is along the streamwise direction, the y-axis is perpendicular to the side walls and the z-axis is normal to the free surface. The origin in this moving coordinate system is located at the intersection between the front wall, the end of the feed zone, and the free surface. The (x, y, z) velocities in the flowing layer are u, v, and w, respectively.

2.2. Validation of DEM simulation: particle distribution compared with experiment

The DEM simulations in this study were validated by comparing the depth dependence of the streamwise velocity and the spatial variation of species concentration to the same quantities obtained from experiments. Agreement between the streamwise velocity profiles obtained in experiments using Particle Tracking Velocimetry (Jain *et al.*, 2002) and simulations was excellent and will be discussed in §3.3 after we present results from simulations.

Figure 3 shows a comparison of final states between DEM simulations and our previous experiments (Fan *et al.*, 2012) for identical conditions with a bidisperse mixture of different-sized particles. We plot the profiles of volume concentration of small particles $c_s = f_s/(f_s + f_l)$ in the steady filling stage along the $x-$direction excluding the flowing layer, where f_s and f_l are the solids volume fraction of small and large particles, respectively. The volume concentration profile for the experiment was obtained using image processing techniques, where the local particle concentration of each species was calculated by first measuring the intensity of each pixel and then calibrating by the intensity of mono-sized particles of each species. Note that the concentration profile measured from the experiment represents the particle distributions at the front glass wall. To measure the concentration profiles in the simulation, the domain was divided into $\Delta x = 1$ cm wide slices in the $x-$direction and averaged in the $y-$direction over particles close to the side wall ($y < 2d_l$) to calculate the volume concentration of each species in each bin. Figure 3 shows that excellent agreement is obtained between the simulations and experiments for a mixture of 1 and 2 mm particles at $\dot{m} = 33$ g/s and $\dot{m} = 120$ g/s. We also found that excellent agreement was obtained between simulations and experiments for other flow rates and particles size distributions. However, from the simulations it is evident that concentration and kinematics vary slightly in the $y-$direction due to wall effects

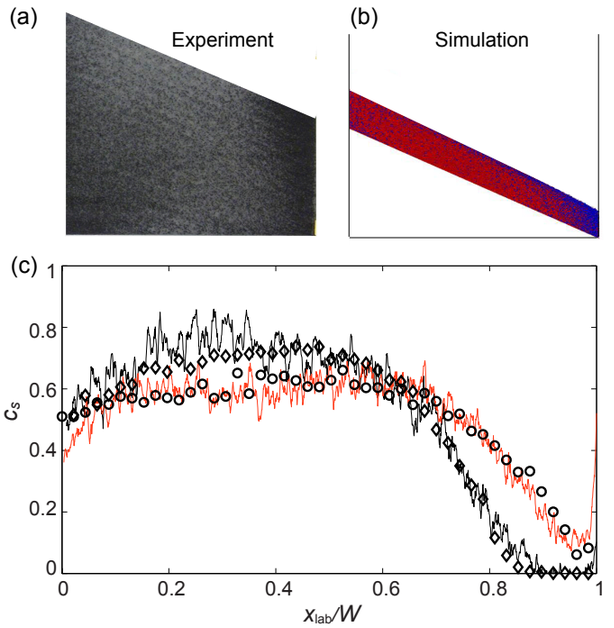

Figure 3. Comparison between experiments and simulations. (a) and (b) show snapshots of segregation patterns in experiments and simulations at the same conditions, respectively. Large particles: black in (a) and blue in (b); small particles: white in (a) and red in (b). (c) Comparison of small particle volume concentration c_s along the $x-$direction between the simulations and the experiments for two different feed rates for 1 mm and 2 mm diameter particles with equal initial mass fractions, where $W = 0.46$ m and $T = 0.013$ m . The black solid curve (experiment) and diamond symbols (simulation) correspond to (a) and (b) where $\dot{m} = 33$ g/s. The red (light) solid curve (experiment) and circle symbols (simulation) correspond to $\dot{m} = 120$ g/s.

(see Appendix 1), which is similar to what occurs in unbounded heap flow (Jop *et al.*, 2005; Katsuragi *et al.*, 2010).

3. Results

3.1. Free surface, dynamic repose angle, and rise velocity

Unlike other free surface granular flows, in bounded heap flow the free surface rises as particles fall onto the heap. Therefore, to measure the time-averaged kinematics such as the velocity profile and thickness of the flowing layer at different locations, the free surface location needs to be determined at each instant of time. To do so, the computational domain is divided into equal, non-overlapping bins of $\Delta x \times \Delta y \times \Delta z$, where $\Delta x = 10$ mm, $\Delta y = T$, and $\Delta z = 0.5$ mm. The local solids volume fraction in each bin was calculated as $f_i = \frac{V_i}{V_{bin}}$, where V_i is the fractional volume of all particles located in bin i, and $V_{bin} = \Delta x \Delta y \Delta z$ is the bin volume. Figure 4(a) shows profiles of solids volume fraction in the $z-$direction at different streamwise locations for a mixture of equal volumes of 1 mm and 2 mm particles for steady flow ($t_0 = 10$ s) at $\dot{m} = 33$ g/s. At each streamwise location, the solids volume fraction is $f \approx 0.65$ in the static portion of the heap for small $z_{\rm lab}$ (for example, in the region $z_{\rm lab} < 0.17$ m for $x_{\rm lab} = 0.1$ m). Moving upward in the heap, the solids volume fraction decreases slightly in the creeping region of the heap due to slow re-arrangement of particles (0.17 m $< z_{\rm lab} <$ 0.185 m for $x_{\rm lab} = 0.1$ m). The solids volume fraction continues to decrease slowly moving upward through the flowing layer (0.185 m $< z_{\rm lab} <$ 0.2 m for $x_{\rm lab} = 0.1$ m). Then the solids volume fraction decreases rapidly to zero close to the free surface. In the upstream region of the heap ($z_{\rm lab} > 0.205$ m for $x_{\rm lab} = 0.1$ m), there is a non-zero solids volume fraction above the free surface, corresponding to the bouncing of some particles after impact on the heap.

Based on the profiles of solids volume fraction, the location of the free surface z_s at each streamwise position can be estimated based on a cutoff value of solids fraction f_c (similar to Freireich *et al.* (2009)). f_c is typically selected at an intermediate value, since too small a value includes bouncing particles in the flowing layer and too large a value includes static particles. In this paper, we use $f_c = 0.35$ because the measured free surface only varies by one particle diameter when f_c is changed between 0.1 and 0.5. The location of the entire free surface at different times is plotted in figure 4(b), indicating a uniformly-sloped surface. The dynamic angle of repose of the heap, α at different times was determined by calculating the slope of the free surface using a linear fit. As shown in the inset of figure 4(b), α remains nearly constant ($25.69 \pm 0.07^\circ$ for the mixture of 1 mm and 2 mm particles at $\dot{m} = 33$ g/s) during the entire course of the steady-state portion of the simulation.

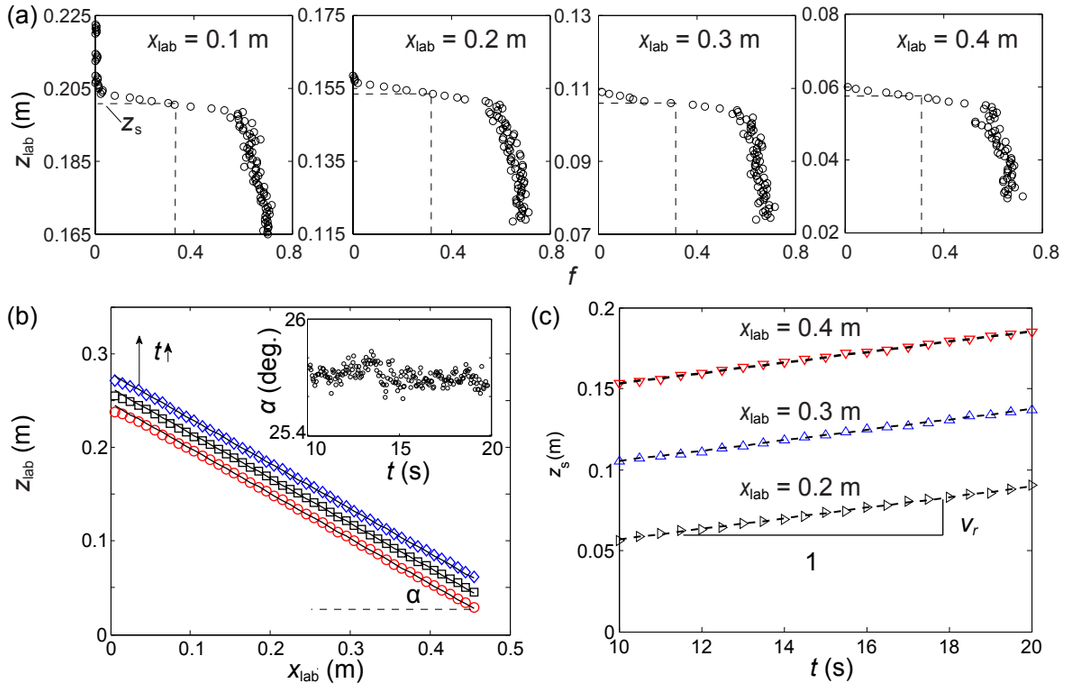

Figure 4. Determining the free surface, dynamic angle of repose and rise velocity. (a) Profiles of solids volume fraction, f, in the $z-$direction at four different $x_{\rm lab}$ location for a mixture of 1 mm and 2 mm particles at $\dot{m} = 33$ g/s and $t_0 = 10$ s, where feed zone is located in the interval $0 < x_{\rm lab} < 8$. Steady flow is achieved at $t_0 = 10$ s. A cutoff value of $f_c = 0.35$ determines the location of the free surface at each x. (b) Free surface at $t = t_0$, $t = t_0 + 2.5$ s, and $t = t_0 + 5$ s from bottom to top. Symbols are data from simulations and lines are linear fits. The angle of repose α at each time is the inverse tangent of the slope of the linear fits. Inset: α as a function of t. (c) z_s at different locations $x_{\rm lab}$ as a function of time. Symbols are data from simulations and lines are linear fits. The slope of the linear fit is the rise velocity, v_r, which is constant across the heap.

When the flow down the heap is continuous (as opposed to intermittently avalanching), the heap rises steadily and uniformly at all positions along the slope. Figure 4(c) shows the free surface z_s as function of time at three different streamwise locations. The linear increase of z_s as a function of time confirms that the free surface rises steadily, as the slope of z_s vs. t is the rise velocity. To facilitate locating the free surface at different times and streamwise locations, we determine the free surface $\tilde{z}_s(x, t_0)$ at the initial time t_0 for the steady state using the linear fit as in figure 4(b). Then the subsequent free surface location at time t is calculated as $\tilde{z}_s(x_{\rm lab}, t) = \tilde{z}_s(x_{\rm lab}, t_0) + v_r(t - t_0)$. The differences between the calculated free surface and measured free surface from simulations $\Delta z_s = \tilde{z}_s(x_{\rm lab}, t) - z_s(x_{\rm lab}, t)$ is $|\Delta z_s/d_s| < 1$ indicating that this approach is accurate.

With the free surface location and the dynamic angle of repose known as a function of time, we can transform from the laboratory $(x_{\rm lab}, y_{\rm lab}, z_{\rm lab})$ to the instantaneous moving reference frame at the free surface (x, y, z). From here on, the kinematics at each time are measured in the coordinates (x, y, z), with corresponding velocity field (u, v, w). The $z-$component of the rise velocity in this coordinate system is $v_r' = v_r \cos\alpha$.

3.2. Kinematics of monodisperse systems

3.2.1. *Streamwise velocity*

We measure the local, time-averaged, streamwise velocity u (and the normal velocity w) by dividing the domain into equal, non-overlapping bins of $\Delta x \times \Delta y \times \Delta z$, where $\Delta x = 10$ mm, $\Delta y = T$, and $\Delta z = 1$ mm. The streamwise velocity in bin i averaged over δt is given by $u_i = \frac{\sum_1^{N_i} V_{ij} u_j}{\sum_1^{N} V_{ij}}$, where V_{ij} is the fractional volume of particle j located in bin i, u_j is the velocity component in the streamwise direction of particle j, and N_i is the total number of particles that are partially or entirely located in bin i during δt. Figure 5(a) shows profiles of u at steady state ($t > t_0$) in the $z-$direction at four different streamwise locations averaged over $\delta t = 10$ s for 1.5 mm monodisperse particles at $\dot{m} = 33$ g/s. The velocity profiles exhibit two regimes: a rapid decrease of u from a maximum value at the free surface in most of the flowing layer and a slow decay to the creeping region near the bottom of the flowing layer. In the quasi-static region below the flowing layer, particles move at small nonzero velocities ($\sim$O(1 mm/s)). The "error" bars in the plots represent the standard deviations of time-averaged u (associated with granular temperature), which show larger standard deviations for larger u, consistent with other results (e.g. Jain *et al.* (2002) in rotating tumblers). The streamwise velocity profiles resemble those in unbounded

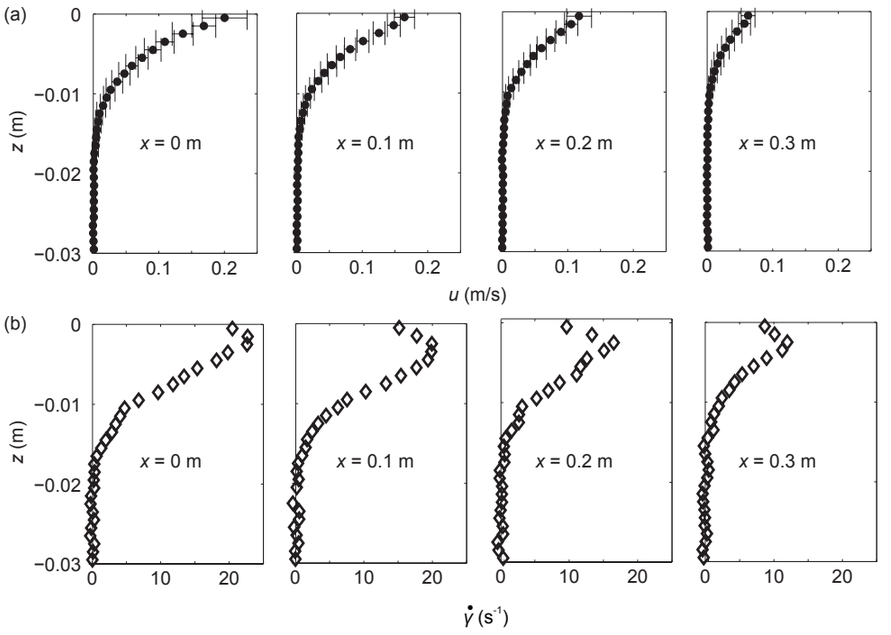

Figure 5. Profiles of streamwise velocity and shear rate in the depth direction, z. (a) Time-averaged steady state streamwise velocity profiles at four different streamwise locations for 1.5 mm monodisperse particles at $\dot{m} = 33$ g/s; error bars indicate the standard deviation of the mean values. (b) Profiles of shear rate $\dot{\gamma} = \partial u/\partial z$ at different streamwise locations as in (a).

heap flow (Komatsu *et al.*, 2001; GDR MiDi, 2004; Jop *et al.*, 2005; Richard *et al.*, 2008; Katsuragi *et al.*, 2010) or rotating tumbler flow (Bonamy *et al.*, 2002; Jain *et al.*, 2002; Hill *et al.*, 2003). However, unlike unbounded heap flow, the streamwise velocity at the same depth z in bounded heap flow decreases in the streamwise direction (as x increases).

Figure 5(b) shows profiles of shear rate $\dot{\gamma} = \partial u/\partial z$ in the depth direction associated with the velocity profiles in figure 5(a). The shear rate at the same depth decreases in the streamwise direction. In a region that is only a few particles thick near the free surface, the shear rate increases slightly to a maximum value as z decreases. Below this region the shear rate decreases smoothly to zero as the static portion of the heap is approached. The shear rate profile in the depth direction is neither constant nor exponential, which indicates that the streamwise velocity profile in the flowing layer is neither linear nor exponential as commonly assumed (Komatsu *et al.*, 2001; GDR MiDi, 2004).

3.2.2. *Kinematics along the streamwise direction*

As mentioned in §1 and unlike the constant flow rate along the streamwise direction in unbounded heap flow or inclined chute flow, the local flow rate in bounded heap flow decreases linearly along the streamwise direction, so kinematic properties, including the surface velocity (u_s), the flowing layer thickness (δ), and average shear rate ($\bar{\dot{\gamma}}$) may change along the streamwise direction.

In figure 6(a), the local, time-averaged, 2D flow rate $q(x) = \int_{z=z_{wall}}^{z=0} u(x,z)dz$ is plotted as a function of x, and shows a linear decrease along the streamwise direction, as expected due to the uniform deposition of material on the heap. The flow rate reaches zero at the downstream bounding endwall at $x = 0.42$ m. Close to $x = 0$, the small deviation from a purely linear decrease is due to a loss of flux as a result of excluding the bouncing particles in the calculation of $q(x)$. Figure 6(b) shows that the velocity at the free surface u_s also decreases approximately linearly in the streamwise direction. The depth-averaged shear rate $\bar{\dot{\gamma}}$ is calculated by averaging the local shear rate $\partial u/\partial z$ over the flowing layer at each x. $\bar{\dot{\gamma}}$ decreases to nearly zero in the streamwise direction as shown in figure 6(c).

To determine the thickness of the flowing layer, it is necessary to locate the bottom of the flowing layer z_{bottom} (or equivalently, the boundary between the flowing layer and the quasi-static region). We tested three different methods to do this based on the streamwise velocity profiles. In the first method, similar to Komatsu *et al.* (2001), Andreotti & Douady (2001), and Courrech du Pont *et al.* (2005), the velocity profile at each streamwise location is fit to $u(x,z) = u_o(x)\exp(z/z_o)$, where u_o is the nominal surface velocity at each x and z_o is a characteristic depth, to which z_{bottom} is proportional. In the second method, the bottom of the flowing layer is determined by extrapolating the approximately linear part of the velocity profile to zero (GDR MiDi, 2004). In the third method, a cutoff value u_c, proportional to u_s at each x (e.g. $0.1u_s$) determines z_{bottom}. Figure 6(d) shows δ as a function

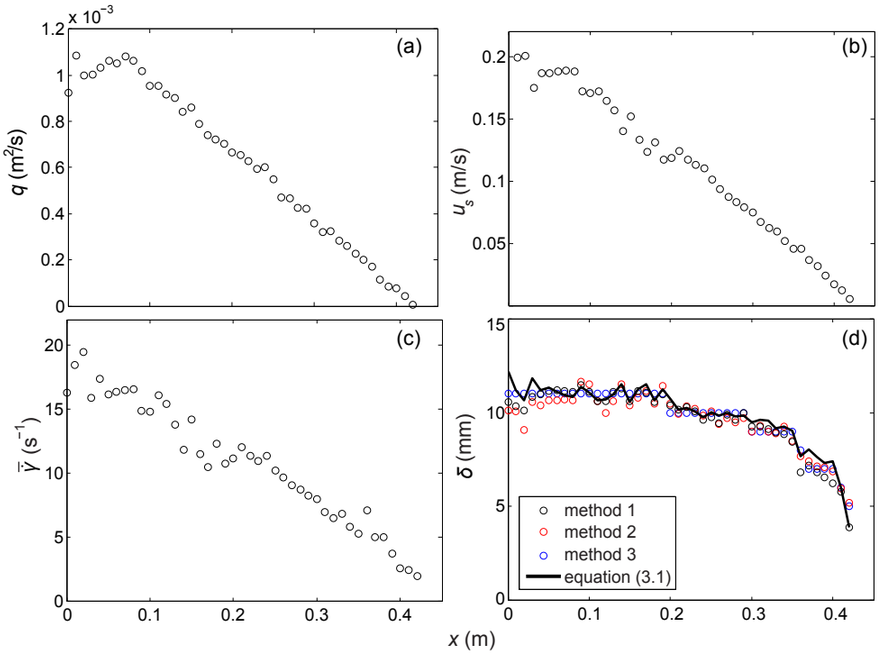

Figure 6. Kinematic parameters vary in the streamwise ($x-$)direction for 1.5 mm particles at $\dot{m} = 33$ g/s. (a) Local 2D flow rate q; (b) streamwise surface velocity u_s; (c) flowing layer averaged shear rate $\overline{\dot{\gamma}}$; (d) flowing layer thickness δ measured using three different methods as described in text. Solid curve is the theoretical prediction from equation 3.1 proposed by Khakhar *et al.* (2001).

of x determined using these three methods. The values calculated for z_{bottom} and, consequently, δ are similar, provided that the appropriate scale factor ($\delta = 2.3 z_o$) for the first method and the cutoff value ($0.1 u_s$) for the third method are used. Similar to other free surface flows, δ spans a few particle diameters ($6d$ to $7d$ for most of the length of the flowing layer shown in figure 6(d)) (Orpe & Khakhar, 2001; Felix *et al.*, 2007; Pignatel *et al.*, 2012). The flowing layer thickness decreases slightly along much of the length of the flowing layer, but decreases somewhat more at the end of the heap.

Khakhar *et al.* (2001) proposed a relation between δ and $\overline{\dot{\gamma}}$ in bounded heap flow along the streamwise direction based on mass conservation:

$$\delta(x) = [\delta_L^2 + 2 v_r (L - x)/\overline{\dot{\gamma}}]^{1/2}, \tag{3.1}$$

where L is the length of the flowing layer and δ_L is the thickness of the flowing layer at $x = L$. Using v_r, $\overline{\dot{\gamma}}$, and δ_L from simulation, we found that δ calculated from equation 3.1 matches the values measured directly from the simulation fairly well, as shown in figure 6(d). However, our results show a decrease of $\overline{\dot{\gamma}}$ along the streamwise direction, contrary to Khakhar *et al.* (2001) where $\overline{\dot{\gamma}}$ was predicted to be constant in the streamwise direction. This discrepancy is possibly due to the measurement technique used by Khakhar *et al.* (2001) to determine δ which they found to decrease along the $x-$direction by manually locating the bottom of the flowing layer using a constant streamwise velocity cutoff instead of the relative value used here.

3.2.3. *Streamwise and normal velocity scaling*

A scaling for streamwise velocity profiles at different streamwise locations is possible by normalizing u by u_s and z by δ at each x so that the streamwise velocity profiles at all streamwise locations collapse onto a single curve, as shown in figure 7(a). Throughout most of the flowing layer ($|z/\delta| < 1$), the scaled velocity u/u_s decreases rapidly from 1 at the free surface. Deeper in the flowing layer, u/u_s decreases approximately exponentially, similar to unbounded heap flow or rotating tumbler flow (Komatsu *et al.*, 2001; GDR MiDi, 2004; Courrech du Pont *et al.*, 2005). This exponential tail can be seen more clearly in figure 7(b), where u/u_s is plotted on a log scale. In deeper regions ($|z/\delta| < 2$) velocities are very small ($|u/u_s| < 0.01$), but nonzero, though there is substantial scatter. Note that in unbounded heap flow or rotating tumbler flow, the velocity can be scaled with $\sqrt{gd}$ at different flow rates (GDR MiDi, 2004), where d is the particle diameter for monodisperse systems. However, since u_s changes with x in bounded heap flow (figure 5(a)), this constant scaling for u is insufficient.

A difference between bounded heap flow and other free surface flows is that particles in the flowing layer have a positive average velocity normal to flow due to the rise of the free surface in the continuous flow regime. For bidisperse flows this positive normal velocity contributes to the separation of small and large particles in the streamwise direction that controls the final segregation state of the heap. This does not occur in other free surface flows due to the unchanging location of the free surface (figure 1). Because of the important role of the vertical

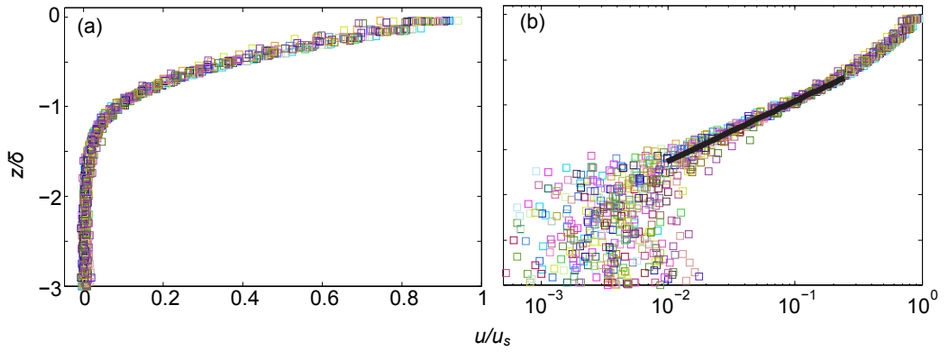

Figure 7. (a) Profiles of u at all x for 1.5 mm particles at $\dot{m} = 33$ g/s, where u is normalized by u_s and z is normalized by δ such that all velocity data fall onto a single curve. Symbols in different colors represent data at different x. (b) Semi-log plot of (a). Solid line is exponential fit $u/u_s = 2.4e^{3.3z/\delta}$ for $-1.6 < z/\delta < -0.7$.

movement of the flowing layer in the final segregation configuration in the bounded heap, an analytical expression for the normal velocity of the heap is useful. To this end, we start with the conservation of mass:

$$\frac{\partial u}{\partial x} + \frac{\partial w}{\partial z} = 0, \tag{3.2}$$

and assume a linear decrease of the streamwise velocity u in the $x-$direction based on the results in §3.2.1 such that to a first approximation:

$$u(x, z) = u(0, z)(1 - x/L), \tag{3.3}$$

where $u(0, z)$ gives the depth dependence at $x = 0$. Substituting equation 3.3 into equation 3.2, integrating with the boundary condition $w = 0$ at $z = 0$ in the moving reference frame, and noting that w is a function of z only (uniform rise of the heap), an expression for the normal velocity $w(z)$ in the flowing layer is obtained:

$$w(z) = \frac{1}{L}\int_z^0 u(0, \xi)d\xi. \tag{3.4}$$

The normal velocity profile can be calculated based on equation 3.4, if $u(0, z)$ is known. Even though the often-used linear or exponential relations do not capture the exact functional form of the streamwise velocity as shown in figure 5(b), we try both forms for $u(0, z)$, a linear expression $u(0, z) = u(0, 0)(1 + z/\delta)$ and an exponential expression $u(0, z) = u(0, 0)\mathrm{e}^{kz/\delta}$, to obtain analytical solutions for the normal velocity. Here, $u(0, 0)$ is the surface velocity at $x = 0$, and k is the ratio of the thickness of the the flowing layer to the characteristic length scale of the exponential fit, where $k = 2.3$ in this study. $u(0, 0)$ is associated with the 2D flow rate q at $x = 0$ by $q_0 = \int_{-\delta}^0 u(0, z)dz$. For the linear streamwise velocity profile, $u(0, 0) = 2q_0/\delta$, and for the exponential streamwise velocity profile, $u(0, 0) = \frac{kq_0}{\delta(1-\mathrm{e}^{-k})}$. Substituting $u(0, 0)$, $q_0 = v_r L$, and $u(0, z)$ into equation 3.4, the normal velocity using the linear streamwise velocity profile is

$$\tilde{w} = 2\tilde{z} + \tilde{z}^2. \tag{3.5}$$

The exponential streamwise velocity profile yields

$$\tilde{w} = \frac{1}{1 - \mathrm{e}^{-k}}\left(\mathrm{e}^{k\tilde{z}} - 1\right), \tag{3.6}$$

where $\tilde{w} = w/v_r'$ and $\tilde{z} = z/\delta$. Note that both equations 3.5 and 3.6 automatically meet the boundary condition that $w = -v_r'$ at $z = -\delta$.

Figure 8 shows theoretical predictions from equations 3.5 and 3.6 (curves), and time-averaged normal velocity measured from simulations in the flowing layer for 1.5 mm particles at $\dot{m} = 33$ g/s at different streamwise locations. Both simulation data and the theoretical curves show that normal velocity in the moving reference frame decreases from zero at the free surface to $-v_r'$ at the bottom of the flowing layer, though the data are somewhat scattered at different streamwise locations due to the stochastic nature of the flow. The theoretical predictions from both equations 3.5 and 3.6 agree with the simulation data, even though some deviations exist. For example, in the upper region of the flowing layer ($|z/\delta| < 0.4$), both analytical solutions slightly underpredict normal velocity. Nonetheless, both analytical solutions provide reasonable predictions for the normal velocity.

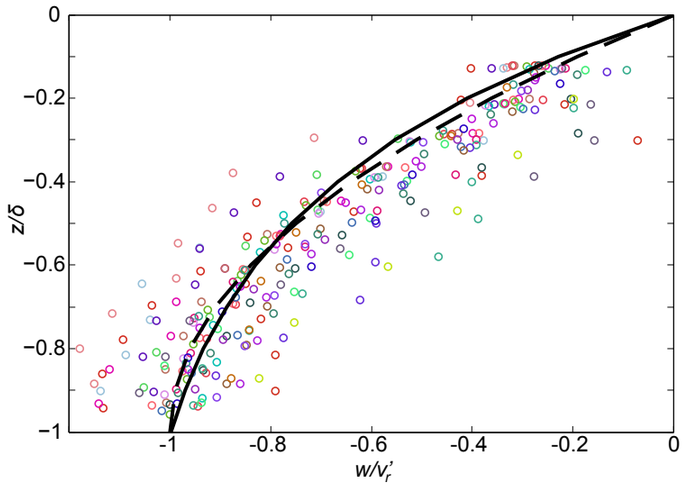

Figure 8. Scaled normal velocity, w/v_r', vs. scaled depth z/δ for 1.5 mm particles at $\dot{m}$=33 g/s. Different color symbols are for $0 < x/L < 1$. Curves show predictions for linear (dashed, equation 3.5) and exponential (solid, equation 3.6) streamwise velocity profiles.

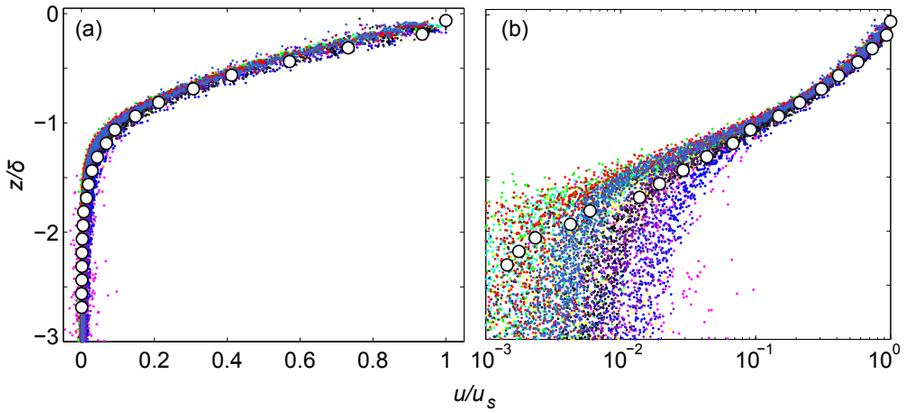

Figure 9. (a) Non-dimensionalized streamwise velocity profiles at different mass feed rates ($10 \leq \dot{m} \leq 120$ g/s), particle size ratios ($1 \leq R \leq 3$), and local particle concentrations ($0 < c_s < 0.9$) from 11 DEM simulations (dots) and one experiment (open circles). (b) Semi-logarithmic plot of (a). Different colors denote different feed rates and particle sizes and size distributions.

3.3. Kinematics at different feed rates and particle size distributions

The results for a monodisperse system with one specific flow rate described in §3.2 demonstrate that the streamwise velocity in bounded heap flow is characterized by the local surface velocity u_s and the thickness of the flowing layer δ (see figure 5), where u_s and δ change along the streamwise direction. However, it is not clear if this scaling is more universally applicable when the feed rate and particle size distributions change. The particle size distribution is characterized by size ratio R ($R = 1$ for the monodisperse systems and $R > 1$ for the bidisperse systems) and particle mean diameters: the local mean particle diameter $\overline{d} = n_s d_s + n_l d_l$, where $n_s = \frac{c_s R^3}{c_s R^3 + c_l}$ and $n_l = \frac{c_l}{c_s R^3 + c_l}$ are the local number fractions, and c_s and c_l are local volume concentrations of small and large particles, respectively.

A total of 11 simulations were performed including four monodisperse systems and seven bidisperse systems with equal volumes of each species, as listed in table 1. The streamwise velocity profiles at different streamwise locations for all these different simulations are plotted in figure 9, where again u is normalized by local surface velocity and z is normalized by local flowing layer thickness. All simulation data collapse onto a single curve in the flowing layer, which is identical to that in figure 7, independent of feed rate and particle size distribution. Clearly, the scaling is valid over a broad range of flow rates and particle size distributions. Furthermore, streamwise velocity profiles from experiments obtained using Particle Tracking Velocimetry[1] show excellent quantitative agreement with the scaled simulation results (open circles in figure 9 are for 3 mm monodispere glass particles at $x/L = 0.5$ and with $\dot{m} = 21$ g/s).

[1] Videos of particle flow in a $36d$ wide by $26d$ high region were acquired at 300 fps using a Casio EX-F1 camera. Before processing, images were shifted vertically so that the free surface was at a fixed location. Then velocity fields were calculated using the Particle Tracking Velocimetry technique (Jain *et al.*, 2002).

Symbol	$\dot{m}$ (g/s)	d_s (mm)	d_l (mm)
◁	10	1.5	–
□	33	1.5	–
◇	91	1.65	–
○	120	1.5	–
▼	10	1	2
▲	33	1	2
◀	120	1	2
▶	33	1.5	3
●	33	1.5	2.25
■	33	1	3
◆	120	1	3

Table 1. Simulation parameters

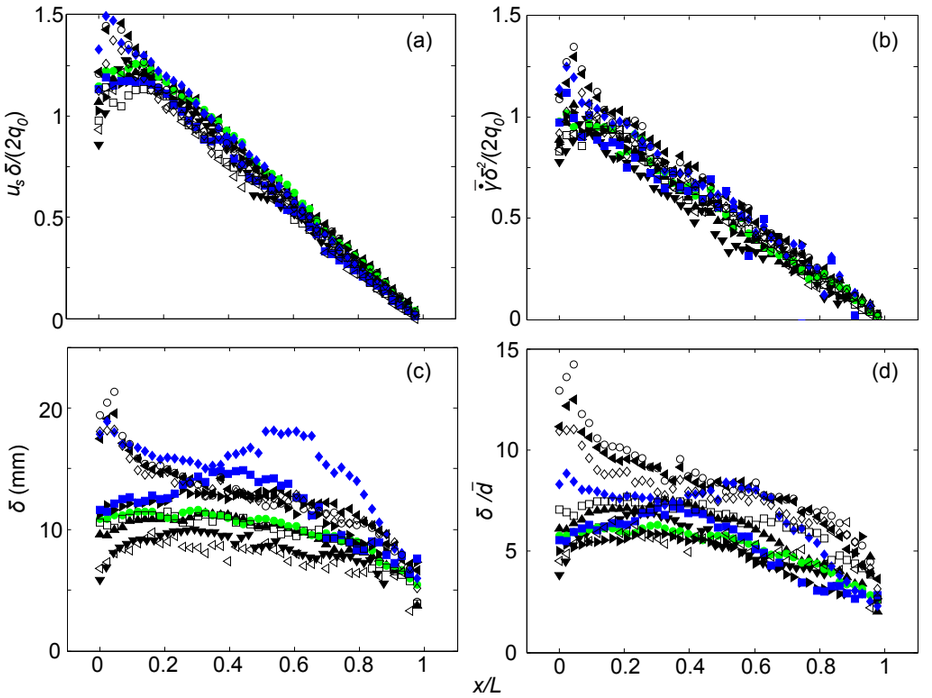

Figure 10. Scaled local kinematic properties at different feed rates and size ratios as listed in table 1. (a) Dimensionless surface velocity $u_s\delta/q_0$ vs. x/L; (b) Normalized average shear rate $\bar{\dot{\gamma}}\delta^2/q_0$ vs. x/L; (c) δ vs. x/L; (d) $\delta/\bar{d}$ vs. x/L. Filled (open) symbols denote bidisperse (monodisperse) systems, see table 1.

We further investigate the dependence of the surface velocity, shear rate, and thickness of the flowing layer along the streamwise direction on the feed rate and the particle size distribution, as shown in figure 10. The surface velocity nondimensionalized by the surface velocity at $x=0$, $u(0,0)=2q_0/\delta$ from §3.2.3, is $u_s\delta/(2q_0)$, which can be plotted along the streamwise direction at all feed rates and particle size distributions. As shown in figure 10(a), plotting $u_s\delta/(2q_0)$ along the streamwise direction collapses the data onto a single curve that decreases linearly along the $x-$direction to the end of the flowing layer, though deviations occur close to the feed zone ($x=0$), probably due to particles bouncing as they fall on the heap. The dimensionless shear rate $\bar{\dot{\gamma}}/(2q_0/\delta^2)$ is plotted in figure 10(b). Again, the data for the different simulation runs collapse onto a single curve, linearly decreasing with x. Since the scaling of u_s and $\bar{\dot{\gamma}}$ depend on the local thickness of the flowing layer δ, how δ varies as flow rates and particle size distributions vary needs further investigation. Figure 10(c) shows δ as a function of x/L at different flow rates and particle size distributions. Except for the regions close to feed zone ($x<0.2$) where particle bouncing effects occur, the flowing layer thickness generally increases as the feed rate increases for the same particle size distribution (namely, the same size ratio and the particle diameter of each component). However, the profiles of the scaled thickness of the flowing layer $\delta/\bar{d}$ in the streamwise direction (figure 10(d)) do not show clear trend when feed rates and particle size distributions are changed.

The dependence of δ on flow rate and particle size has been studied in other free surface flows such as rotating tumbler flow or unbounded heap flow for monodisperse systems (e.g. GDR MiDi (2004); Renouf *et al.* (2005); Pignatel *et al.* (2012) and references therein). In all cases, $\delta/\bar{d}\propto(q^*)^a$, where $q^*=q/(\bar{d}\sqrt{g\bar{d}})$ is the dimensionless

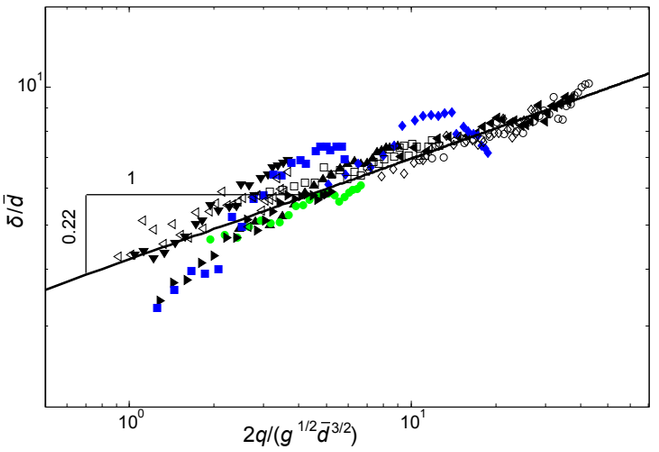

Figure 11. $\delta/\bar{d}$ vs. normalized local 2D flow rate $2q/(g^{1/2}\bar{d}^{3/2})$. Symbols are defined in table 1.

flow rate. In figure 11, we plot $\delta/\bar{d}$ as a function of the local q^* for $x/L \geq 0.2$ on a log-log scale and find that data from all simulations appear to follow a power law relation between $\delta/\bar{d}$ and q^* with $a \approx 0.22$. This value for a differs from that reported by GDR MiDi (2004) and Renouf *et al.* (2005), where $a \approx 0.5$, but is close to what Pignatel *et al.* (2012) found at comparable q^* in rotating tumblers, where a ranged from 0.1 to 0.45. Perhaps what is most important here is that figure 11 can be used to predict the flowing layer thickness, at least approximately, over a wide range of flow rates and particle sizes.

4. Discussions and conclusions

We have shown that streamwise velocity profiles in continuous, bounded, heap flow at different feed rates and particle size distributions collapse onto a single curve when u is scaled by the local surface velocity u_s and depth is scaled by the local flowing layer thickness δ (figure 9), where u_s depends on the feed rate q and δ (figure 10(a)). This result demonstrates a universal functional form for the streamwise velocity in bounded heap flow for both monodisperse and bidisperse systems with the local flowing layer thickness being the only scaling parameter at a given feed rate. The fact that streamwise velocity profiles are independent of the local particle size distributions associated with segregation of bidisperse particles along the streamwise direction is different from other free surface flows such as inclined chute flow (Rognon *et al.*, 2007; Tripathi & Khakhar, 2011) or rotating tumbler flow (Hill & Zhang, 2008). Specifically, Rognon *et al.* (2007) found that in bidisperse systems the segregating larger particles in the upper portion of the flowing layer have a smaller velocity as they slide over the smaller particles in the lower portion of the flowing layer, which results in a different velocity profile from a monodisperse system. Tripathi & Khakhar (2011) further showed that varying the local concentration of large particles can result in a non-monotonic change of streamwise velocity, where a minimum streamwise velocity occurs at a mass fraction of 70% large particles. They also showed that velocity profiles depend on the size ratio of the two species. Although it was not explicitly stated, Hill & Zhang (2008) showed that in a rotating tumbler with a bidisperse mixture, the streamwise velocities at the upper portion of the flowing layer decrease as more large particles segregate to this region. The underlying mechanism for the different effects of particle size distribution on the streamwise velocity between bounded heap flow and other free surface flows is not clear, but might be associated with the linear decrease in local flow rate due to uniform particle deposition into the static bed. For certain parameter values, this effect seems to dominate over the different mobilities of large and small particles in the flow when they segregate.

As we have discussed, the flowing layer thickness can be determined from the velocity profile using any of several techniques as shown in §3.2.2. However, our results demonstrate that the flowing layer thickness as a scaling parameter is insensitive to the specific functional form of the streamwise velocity profile and the specific measurement approach. The local flowing layer thickness depends only on the local flow rate and the local average particle diameter (figure 11). For a monodisperse system, the velocity field is well defined by these two variables. For a bidisperse system, however, local mean particle diameter changes as segregation occurs, so determining the streamwise velocity for bidisperse system requires a prediction of the local concentration of each species.

Although we have found a scaling for the streamwise velocity in bounded quasi 2D heap flow, a specific functional form has not yet been determined. A non-monotonic local shear rate in the depth-direction results in the streamwise velocity that is neither linear nor exponential. To determine the streamwise velocity profile theoretically, a constitutive law that determines the stress is necessary. With recent substantial progress on the rheology of dense granular flow, a local rheological model like that proposed by Jop *et al.* (2006) or a non-local

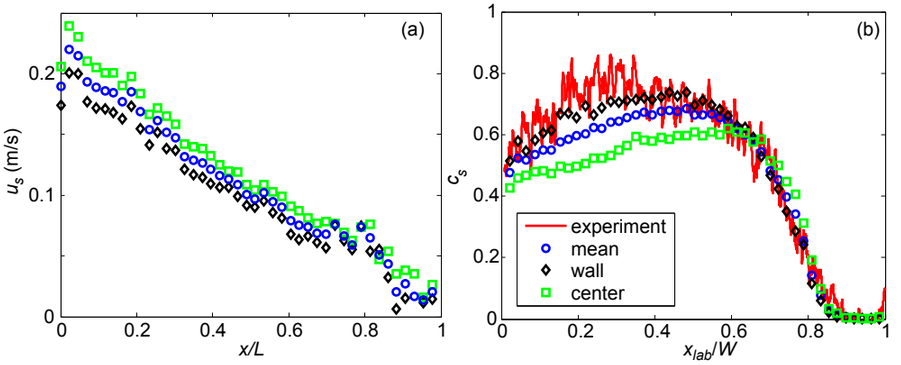

Figure A.12. Side wall effects on kinematics and segregation in bidisperse quasi-2D bounded heap flow. (a) Profiles of surface velocity in the streamwise direction averaged over different portions of the gap between sidewalls in the lateral (y) direction: $0 < y < 4$ mm and $8.7 < y < 12$ mm (wall), $4 < y < 8.7$ mm (center), and $0 < y < 12.7$ mm (mean). (b) Profiles of mass concentration of small particles along the streamwise directions averaged over different portions of the gap in the lateral direction. The data are for a mixture of 1 and 2 mm particles at $\dot{m} = 33$ g/s.

model like that proposed by Kamrin & Koval (2012) might be adapted to bounded heap flow. Subsequently, the normal velocity could be obtained based on mass conservation. However, without an exact expression for the streamwise velocity, assuming a linear or an exponential streamwise velocity profile, similar to previous studies in other free surface flows (e.g. GDR MiDi (2004) and reference therein), gives expressions for the normal velocity that match the simulation data equally well.

The mean flow kinematics of the bidisperse granular systems presented here provide a necessary precursor for modeling segregation in bounded heap flow. The motion of each species in the segregating mixture can be determined by superposing the relative motion of the species – the segregation velocity – onto the mean flow. Thus, the local concentration of each species can be determined using the transport equation for each species and considering the combined effects of advective fluxes related to the mean flow, the segregation fluxes, and the diffusive fluxes due to particle collisions. This approach has been used to model size segregation in other free surface flows, such as inclined chute flow (Dolgunin & Ukolov, 1995; Savage & Lun, 1988; Gray & Thornton, 2005; Gray *et al.*, 2006). However, in these studies, the kinematics are relatively simple: the flow is fully-developed ($\partial u/\partial x = 0$), mean flow has no normal component ($w = 0$), and the streamwise velocity profile is linear. In contrast, bounded heap flow is more complicated in that the mean flow decelerates in the streamwise direction ($\partial u/\partial x < 0$) and the normal velocity profile is non-zero and non-linear. As a result, the advection of each species associated with mean flow may become important, and the shear rate could influence the segregation velocity of each species (May *et al.*, 2010; Marks *et al.*, 2011; Fan & Hill, 2011*b*) and the diffusion coefficients (Utter & Behringer, 2004). These effects might also need to be included when modeling segregation in bounded heap flow.

5. Acknowledgements

We are grateful for helpful discussions with Karl Jacob and Ben Freireich. We also acknowledge financial support from The Dow Chemical Company.

Appendix 1 Wall effects

In quasi-2D unbounded heap flow or inclined chute flow, the side walls significantly influence flow kinematics and rheology (Jop *et al.*, 2005; Katsuragi *et al.*, 2010). Particles are slowed down due to wall friction resulting in a blunt velocity profile with slight decrease of the velocity close to the side walls. In bounded heap flow, the side walls have a similar effect on the streamwise velocity. Figure A.12(a) shows the streamwise surface velocity u_s averaged over different portions of the gap between side walls to investigate wall effects. Although surface velocities in different portions of the gap exhibit a similar linear decrease in the streamwise direction, surface velocities close to the wall (data averaged over 4 mm thick slices in the $y-$direction adjacent to both side walls) are roughly 10% smaller than mean surface velocities, while those in the central region of the heap ($4 < y < 8.7$ mm) are 10% larger. Furthermore, the strength of segregation is also affected by the side walls. As shown in figure A.12(b), the profiles of volume concentration of small particles c_s in the streamwise direction show that segregation strengthes close to side walls. Although c_s decreases from the side walls to the center in the upstream region of the heap ($x_{\rm lab}/W < 0.6$), c_s does not vary in the spanwise direction in the downstream region. This indicates that a small degree of horizontal segregation occurs in the lateral direction, presumably since small

particles segregate toward the side walls due to wall exclusion of large particles or shear-induced segregation (Fan & Hill, 2011*a*). In this work, we report kinematic quantities averaged over the entire gap ($0 < y < T$), since the wall effects are relatively small.

References

ABATE, A. R., KATSURAGI, H. & DURIAN, D. J. 2007 Avalanche statistics and time-resolved grain dynamics for a driven heap. *Phys. Rev. E* **76**, 061301.

ANDREOTTI, B. & DOUADY, S. 2001 Selection of velocity profile and flow depth in granular flows. *Phys. Rev. E* **63**, 031305,1–8.

BAXTER, J., TÜZÜN, U., HEYES, D., HAYATI, I. & FREDLUND, P. 1998 Stratification in poured granular heaps. *Nature* **391**, 136.

BENITO, J. G., IPPOLITO, I. & VIDALES, A. M. 2013 Novel aspects on the segregation in quasi 2d piles. *Powder Technology* **234**, 123 – 131.

BONAMY, D., DAVIAUD, F. & LAURENT, L. 2002 Experimental study of granular surface flows via a fast camera: A continuous description. *Physics of Fluids* **14** (5), 1666–1673.

BOUTREUX, T. & DE GENNES, P.-G. 1996 Surface flows of granular mixtures, i. general principles and minimal model. *J. Phys. I* **6**, 1295.

BOUTREUX, T., RAPHAËL, E. & DE GENNES, P.-G. 1998 Surface flows of granular materials: a modified picture for thick avalanches. *Phys. Rev. E* **58**, 4692–4700.

BRIDGWATER, J., COOKE, M. H. & SCOTT, A. M. 1978 Interparticle percolation: equipment development and mean percolation velocities. *Trans. Inst. Chem. Engrs.* **56**, 157.

CHEN, P., OTTINO, J. M. & LUEPTOW, R. M. 2008 Subsurface granular flow in rotating tumblers: A detailed computational study. *Phys. Rev. E* **78**, 021303.

CHEN, P., OTTINO, J. M. & LUEPTOW, R. M. 2011 Granular axial band formation in rotating tumblers: a discrete element method study. *New J. Phys.* **13**, 055021.

COOKE, M. H., BRIDGWATER, J. & SCOTT, A. M. 1978 Interparticle percolation: Lateral and axial diffusion coefficients. *Powder Technol.* **21**, 183.

CRASSOUS, J., METAYER, J-F, RICHARD, P. & LAROCHE, C. 2008 Experimental study of a creeping granular flow at very low velocity. *Journal of Statistical Mechanics: Theory and Experiment* **2008** (03), P03009.

CUNDALL, P. A. & STRACK, O. D. L. 1979 A discrete numerical model for granular assemblies. *Geotechnique* **29**, 47–65.

DOLGUNIN, V.N. & UKOLOV, A.A. 1995 Segregation modeling of particle rapid gravity flow. *Powder Technology* **83** (2), 95 – 103.

DRAHUN, J. A. & BRIDGWATER, J. 1983 The mechanisms of free surface segregation. *Powder Technol.* **36**, 39–53.

FAN, Y., BOUKERKOUR, Y., BLANC, T., UMBANHOWAR, P. B., OTTINO, J. M. & LUEPTOW, R. M. 2012 Stratification, segregation, and mixing of granular materials in quasi-two-dimensional bounded heaps. *Phys. Rev. E* **86**, 051305.

FAN, Y. & HILL, K. M. 2011*a* Phase transitions in shear-induced segregation of granular materials. *Phys. Rev. Lett.* **106**, 218301.

FAN, Y. & HILL, K. M. 2011*b* Theory for shear-induced segregation of densegranular mixtures. *New J. Phys.* **13**, 095009.

FELIX, G., FALK, V. & D'ORTONA, U. 2007 Granular flows in a rotating drum: the scaling law between velocity and thickness of the flow. *The European Physical Journal E* **22**, 25–31.

FREIREICH, B., LITSTER, J. & WASSGREN, C. 2009 Using the discrete element method to predict collision-scale behavior: A sensitivity analysis. *Chem. Eng. Sci.* **64**, 3407–3416.

GDR MIDI 2004 On dense granular flows. *Eur. Phys. J. E* **14**, 341.

GOUJON, C., DALLOZ-DUBRUJEAUD, B. & THOMAS, N. 2007 Bidisperse granular avalanches on inclined planes: A rich variety of behaviors. *The European Physical Journal E* **23**, 199–215.

GOYAL, R. K. & TOMASSONE, M. S. 2006 Power-law and exponential segregation in two-dimensional silos of granular mixtures. *Phys. Rev. E* **74**, 051301.

GRAY, J.M.N.T. & ANCEY, C. 2009 Segregation, recirculation and deposition of coarse particles near two-dimensional avalanche fronts. *J. Fluid Mech.* **629**, 387–423.

GRAY, J. M. N. T. & HUTTER, K. 1997 Pattern formation in granular avalanches. *Continuum Mechanics and Thermodynamics* **9**, 341–345.

GRAY, J. M. N. T., SHEARER, M. & THORNTON, A. R. 2006 Time-dependent solutions for particle-size segregation in shallow granular avalanches. *Proc. R. Soc. A* **462**, 947–972.

GRAY, J. M. N. T. & THORNTON, A. R. 2005 A theory for particle size segregation in shallow granular free-surface flows. *Proc. R. Soc. A* **461**, 1447.

HILL, K. M., GIOIA, G. & TOTA, V. V. 2003 Structure and kinematics in dense free-surface granular flow. *Phys. Rev. Lett.* **91**, 064302.

HILL, K. M. & ZHANG, J. 2008 Kinematics of densely flowing granular mixtures. *Phys. Rev. E* **77**, 061303.

JAIN, N., OTTINO, J. M. & LUEPTOW, R. M. 2002 An experimental study of the flowing granular layer in a rotating tumbler. *Physics of Fluids* **14** (2), 572–582.

JOP, P., FORTERRE, Y. & POULIQUEN, O. 2005 Crucial role of sidewalls in granular surface flows: consequences for the rheology. *J. Fluid Mech.* **541**, 167–192.

JOP, P., FORTERRE, Y. & POULIQUEN, O. 2006 Kinematics of densely flowing granular mixtures. *Nature (London)* **441**, 727–730.

KAMRIN, K. & KOVAL, G. 2012 Nonlocal constitutive relation for steady granular flow. *Phys. Rev. Lett.* **108**, 178301.

KATSURAGI, H., ABATE, A. R. & DURIAN, D. J. 2010 Jamming and growth of dynamical heterogeneities versus depth for granular heap flow. *Soft Matter* **6**, 3023–3029.

KHAKHAR, D. V., MCCARTHY, J. J., SHINBROT, TROY & OTTINO, J. M. 1997 Transverse flow and mixing of granular materials in a rotating cylinder. *Physics of Fluids* **9** (1), 31–43.

KHAKHAR, D. V., ORPE, A. V., ANDERSÉN, P. & OTTINO, J. M. 2001 Surface flow of granular materials: model and experiments in heap formation. *J. Fluid Mech.* **441**, 255–264.

KOEPPE, J. P., ENZ, M. & KAKALIOS, J. 1998 Phase diagram for avalanche stratification of granular media. *Phys. Rev. E* **58**, R4104–R4107.

KOMATSU, T. S., INAGAKI, S., NAKAGAWA, N. & NASUNO, S. 2001 Creep motion in a granular pile exhibiting steady surface flow. *Phys. Rev. Lett.* **86**, 1757–1760.

LEMIEUX, P.-A. & DURIAN, D. J. 2000 From avalanches to fluid flow: A continuous picture of grain dynamics down a heap. *Phys. Rev. Lett.* **85**, 4273–4276.

LINARES-GUERRERO, E., GOUJON, C. & ZENIT, R. 2007 Increased mobility of bidisperse granularavalanche. *J. Fluid Mech.* **593**, 475–504.

MAKSE, H. A., CIZEAU, P. & STANLEY, H. E. 1997*a* Possible stratification mechanism in granular mixtures. *Phys. Rev. Lett.* **78**, 3298.

MAKSE, H. A., HAVLIN, S., KING, P. R. & STANLEY, H. E. 1997*b* Spontanenous stratification in granular mixtures. *Nature* **386**, 379.

MARKS, B., ROGNON, P. & EINAV, I. 2011 Grainsize dynamics of polydisperse granular segregation down inclined planes. *J. Fluid Mech.* **690**, 499.

MAY, L. B. H., GOLICK, L. A., PHILLIPS, K. C., SHEARER, M. & DANIELS, K. E. 2010 Shear-driven size segregation of granular materials: Modeling and experiment. *Phys. Rev. E* **81**, 051301.

MEIER, S. W., LUEPTOW, R. M. & OTTINO, J. M. 2007 A dynamical systems approach to mixing and segregation of granular materials in tumblers. *Advances in Physics* **56** (5), 757–827.

ORPE, A. V. & KHAKHAR, D. V. 2001 Scaling relations for granular flow in quasi-two-dimensional rotating cylinders. *Phys. Rev. E* **64**, 031302.

OTTINO, J.M. & KHAKHAR, D.V. 2000 Mixing and segregation of granular materials. *Annu. Rev. Fluid Mech.* **32**, 55.

PIGNATEL, F., ASSELIN, C., KRIEGER, L., CHRISTOV, I. C., OTTINO, J. M. & LUEPTOW, R. M. 2012 Parameters and scalings for dry and immersed granular flowing layers in rotating tumblers. *Phys. Rev. E* **86**, 011304.

COURRECH DU PONT, S., FISCHER, R., GONDRET, P., PERRIN, B. & RABAUD, M. 2005 Instantaneous velocity profiles during granular avalanches. *Phys. Rev. Lett.* **94**, 048003.

POULIQUEN, O. & FORTERRE, Y. 2002 Friction law for dense granular flows: application to the motion of a mass down a rough inclined plane. *J. Fluid Mech.* **453**, 133–151.

RAHMAN, M., SHINOHARA, K., ZHU, H.P., YU, A.B. & ZULLI, P. 2011 Size segregation mechanism of binary particle mixture in forming a conical pile. *Chem. Eng. Sci.* **66**, 6089.

RAPAPORT, D. C. 2002 Simulational studies of axial granular segregation in a rotating cylinder. *Phys. Rev. E* **65**, 061306.

RENOUF, M., BONAMY, D., DUBOIS, F. & ALART, P. 2005 Numerical simulation of two-dimensional steady granular flows in rotating drum: On surface flow rheology. *Physics of Fluids* **17** (10), 103303.

RICHARD, P., VALANCE, A., MÉTAYER, J.-F., SANCHEZ, P., CRASSOUS, J., LOUGE, M. & DELANNAY, R. 2008 Rheology of confined granular flows: Scale invariance, glass transition, and friction weakening. *Phys. Rev. Lett.* **101**, 248002.

RISTOW, G. H. 2000 Pattern formation in granular materials. Berlin: Springer.

ROGNON, P. G., ROUX, J.-N., NAAIM, M. & CHEVOIR, F. 2007 Dense flows of bidisperse assemblies of disks down an inclined plane. *Phys. Fluids* **19** (5), 058101.

DE RYCK, A., ZHU, H. P., WU, S. M., YU, A. B. & ZULLI, P. 2010 Numerical and theoretical investigation of the surface flows of granular materials on heaps. *Powder Technol.* **203**, 125–132.

SAVAGE, S. B. & HUTTER, K. 1989 The motion of a finite mass of granular material down a rough incline. *J. Fluid Mech.* **199**, 177–215.

SAVAGE, S. B. & LUN, C. K. K. 1988 Particle size segregation in inclined chute flow of dry cohesionless granular solids. *J. Fluid Mech.* **189**, 311.

SCHAFER, J., DIPPEL, S. & WOLF, D. E. 1996 Force schemes in simulations of granular materials. *J. Phys. I France* **6**, 5–20.

SHINOHARA, K. & ENSTAD, G. 1990 Segregation mechanism of binary solids in filling axi-symmetric hoppers. p. 45. Proceedings of Second World Congress Particle Technology, Kyoto.

SHINOHARA, K., SHOJI, K. & TANAKA, T. 1972 Mechanism of size segregation of particles in filling a hopper. *Ind. Eng. Chem. Process Des. Dev.* **11**, 369.

SILBERT, L. E., GREST, G. S., BREWSTER, R. & LEVINE, A. J. 2007 Rheology and contact lifetimes in dense granular flows. *Phys. Rev. Lett.* **99**, 068002.

THOMAS, N. 2000 Reverse and intermediate segregation of large beads in dry granular media. *Phys. Rev. E* **62** (1), 961–974.

TRIPATHI, A. & KHAKHAR, D. V. 2011 Rheology of binary granular mixtures in the dense flow regime. *Phys. Fluids* **23** (11), 113302.

UTTER, B. & BEHRINGER, R. P. 2004 Self-diffusion in dense granular shear flows. *Phys. Rev. E* **69**, 031308.

WIEDERSEINER, S., ANDREINI, N., EPELY-CHAUVIN, G., MOSER, G., MONNEREAU, M., GRAY, J. M. N. T. & ANCEY, C. 2011 Experimental investigation into segregating granular flows down chutes. *Phys. Fluids* **23**, 013301.

WILLIAMS, J. C. 1963 The segregation of powders and granular materials. *Univ. Sheffield Fuel Soc. J.* **14**, 29.

WILLIAMS, J. C 1968 The mixing of dry powders. *Powder Technol.* **2**, 13–20.